Detailed analysis of combustion stability in a spark-assisted compression ignition engine under nearly stoichiometric and heavy EGR conditions

Detailed analysis of combustion stability in a spark-assisted compression ignition engine under nearly stoichiometric and heavy EGR conditions

Jacek Hunicz[1),*], Maciej Mikulski[2)], Grzegorz Koszałka[1)], Piotr Ignaciuk[1)]

[1)] Lublin University of Technology, Faculty of Mechanical Engineering, Nadbystrzycka 36, 20-618 Lublin, Poland

[2)] University of Vaasa, School of Technology and Innovation, Wolffintie 34, FI-65200 Vaasa, Finland

* E-mail: j.hunicz@pollub.pl

Abstract

Extending the load range of low-temperature combustion is of priority to meet future CO_2 and emission targets for reciprocating engine applications. Spark assist is a feasible solution to this challenge for mono-fuel homogeneous charge compression ignition (HCCI). This paper explains how spark-assisted compression ignition (SACI) enables ultra-low NO_X targets to be met, with acceptable pressure rise rates and combustion stability, at high load boundary conditions, favourable for HCCI/SACI transition. The work provides new methods of combustion analysis which give better understanding of the mechanisms and their implementation for real-time control of SACI engines. The goals are achieved by a combination of single-cylinder engine research and high-fidelity/high-speed, model-based calculations, performed on an individual cycle basis. The results show that determining the start of the kinetic phase in SACI is possible via standard combustion indicators. The new method is two orders of magnitude faster than the commonly used spline-Wiebe approach. With real-time capability and proven correlation to temperature evolution, triggered by propagating flame, the method enables in-cycle predictive control. Additionally, it gives a deeper insight of the mechanisms underpinning the demonstrated superior performance. The study shows the capability to run SACI at indicated mean effective pressure (IMEP) of 0.5 MPa with engine-out NO_X below Euro VI´s heavy-duty engine limit and with specific fuel consumption of 207 g/kWh. Importantly, pressure rise rate and variation in IMEP do not exceed 0.25 MPa/CAD and 3% respectively. Margins for critical parameters are far greater than for baseline autonomous HCCI, providing significant load extension potential.

Nomenclature

CA – crank angle

CA05, CA50, CA95 – crank angle of 5%, 50% and 95% of the cumulative heat release respectively

CA05-95, CA05-50, CA50-95 – combustion duration between CA05 and CA95, CA05 and CA50 and CA50 and CA95, respectively

CAD – crank angle degree

CASP – crank angle at spark discharge

CCV – cycle-to-cycle variation

CHR – cumulative gross heat release

CO_2 – carbon dioxide

CoV – coefficient of variation

EGR – exhaust gas recirculation

EOC – end of combustion

FTIR – Fourier transform infrared

HCCI – homogeneous charge compression ignition

HRR – heat release rate

I-EGR – internal exhaust gas recirculation

IMEP – indicated mean effective pressure

ISFC – indicated specific fuel consumption

IVC – intake valve closing

LTC – low temperature combustion

m_A – mass of air

m_{EGR} – mass of recirculated exhaust

m_F – mass of fuel

MAP – manifold absolute pressure

MFB – mass fraction burnt

NO_X – nitrogen oxides

NVO – negative valve overlap

p – pressure

PM – particulate matter

PRR – pressure rise rate

rpm – revolutions per minute

SA – spark advance

SACI – spark-assisted compression ignition

SI – spark ignition

SOC – start of combustion

SOI – start of injection

STD – standard deviation

TDC – top dead centre

V – volume

α – actual crank angle degree
γ – ratio of specific heats
λ – excess air ratio
Φ – fuel-charge equivalence ratio

1. Introduction

Manufacturers of road vehicles and other machinery powered by internal combustion engines are under enormous pressure to reduce the environmental impact of their products [1]. Tank-to-wheels emission of CO_2 can be reduced by increasing engine thermal and mechanical efficiency, while introducing biofuels or electrofuels can help to reduce well-to-tank emissions. Apart from the CO_2 issue, emissions of toxic exhaust compounds, in particular nitrogen oxides (NO_X) and particulate matter (PM), still pose a challenge for contemporary combustion engines [2], [3]. One solution, homogeneous charge compression ignition (HCCI), provides high thermal efficiency with low NO_X and PM emissions. HCCI´s volumetric combustion of a highly diluted mixture greatly reduces local in-cylinder temperatures. Low combustion temperature prevents NO_X formation, while lean mixture does not support PM formation [4].

There are several ways of achieving HCCI of fuels with a high octane number. All rely on controllable introduction of thermal energy into the cylinder, aiming for ignition of the fuel mixture at the desired crank angle (CA). The methods include fast thermal management [5], [6] or internal exhaust gas recirculation (I-EGR) through negative valve overlap (NVO) [7]. Using variable valve actuation, NVO provides in-cycle control of the amount of residuals trapped in the cylinder via early closing of the exhaust valve. With late opening of the intake valve, the residuals are recompressed during the NVO period. This recompression of the in-cylinder gas trapped between exhaust and intake strokes provides energy necessary for auto-ignition of fuels like gasoline, despite the low compression ratio of spark-ignition engines [4], [8]. Maintaining this compression ratio is crucial for the transition to positive valve overlap and conventional spark ignition (SI) operation [9]. This transition is needed to address the limited load range of HCCI mode in practical applications. High engine-load is limited in HCCI by excessive peak combustion pressure and pressure rise rates [10], [11]. NVO poses additional constraints in that respect because I-EGR limits fresh air aspiration.

Auto-ignition in an HCCI engine is spontaneous and governed by mixture reactivity and temperature [12], which are constituted at intake valve closing (IVC). Although HCCI

combustion under favourable conditions is considered stable, it can exhibit significant cycle-to-cycle variation (CCV) related to the lack of direct ignition control [13]. Interestingly, HCCI combustion using NVO has some self-regulation, because the moment of auto-ignition and the thermal state of the gas trapped in the previous cycle are directly related [14], [15]. Koopmans et al. [16] explained the CCV mechanism in NVO-induced HCCI as a coupling of combustion timing, residual composition and IVC temperature. Late combustion phasing produces more unburnt hydrocarbons due to expansion-driven rapid temperature drop and resulting combustion quenching. These hydrocarbons remain during the NVO recompression, and for lean combustion cases, can reignite in this phase. This increases the temperature of the residuals transferred to the next cycle, shortening ignition delay. Early phasing leads to low HC emissions and the whole cycle repeats, producing oscillations in combustion phasing, associated peak pressure and heat release rate (HRR). HCCI´s CCV mechanism was confirmed by Hellström et al. [12], [17]. Interestingly, Ebrahimi and Desmet [18] observed pronounced cycle-to-cycle coupling in an engine with positive valve overlap. Nevertheless, its explanation was the same as in the above-mentioned NVO studies. Even small amounts of trapped residuals, attributed to this valving strategy, were enough to transfer effective portions of exhaust reactive species from an incomplete cycle to the following one.

CCV in HCCI usually increases at low engine-loads due to high fuel dilution, either by air or recirculated exhaust. On the other hand, high-load operation is also associated with high CCV because at high amounts of fresh air, reduced amounts of trapped residuals can hardly provide enough energy for the mixture to auto-ignite. HCCI´s operational window can be extended by injecting some part of the fuel directly into the cylinder during the NVO phase. In residually-affected HCCI, the NVO-injected fuel is subjected to evaporation, reformation and partial oxidation, affecting both temperature and mixture reactivity at IVC [19], [20]. Because of this synergy between thermal and chemical effects, cycle-to-cycle coupling becomes much more complex, resulting in periodic combustion parameter oscillations. Early and late combustion events occurring interchangeably from cycle to cycle were observed, among others, by Hunicz et al. [21]. This was typical for the lean mixture enabling partial fuel reformation during NVO. For stoichiometric mixture, variability became stochastic in nature, rather than deterministic.

Finally, it should be noted that much effort has been directed at predicting and actively suppressing HCCI combustion variability. Ghazimirsaied and Koch [22] elaborated a real-time method for predicting combustion timing in individual cycles. They used it to control the blend ratio of two fuels with different octane numbers, and thus correct combustion timing

oscillations. Lawler et al. [23] proposed water injection to control start of combustion and its rate on cycle-to-cycle basis. Wick et al. [24] built model-based HCCI control algorithms able to predict misfires and used spark re-ignition as a preventive tool.

This study proposes spark-assisted compression ignition (SACI) to provide additional HCCI combustion control. SACI is an intermediate concept, comprising flame development initiated by spark discharge, followed by HCCI kinetic combustion. Kalian et al. [25] demonstrated that spark assistance helps to set optimal combustion timing with only slight increase in NO_X emissions. However, spark timing´s effect on burn duration was non-monotonic. Optical investigations by Aleiferis et al. [26] revealed that the flame kernel acted as a "hot spot" rather than increasing bulk in-cylinder temperature.

Adding a spark discharge improves combustion stability in terms of indicated mean effective pressure (IMEP) [25]. However, in the highly diluted mixtures that support ultra-low emissions in HCCI, spark-induced flame propagation is slow and more variable than with conventional SI combustion [27]. Therefore, at such conditions, combustion phasing remains very unstable in SACI [28]. The variable amounts of fuel burnt by flame propagation is the cause of changes in combustion timing. The bigger the SI fraction, the earlier the rapid kinetic combustion phase starts. This coupling is valid both on the different operating point basis as well as on the individual cycle basis. The latter mechanism governs the CCV in SACI.

Daw et al. [29] analysed cyclic variations of heat release for highly diluted mixture. They indicated that CCV dynamics for autonomous HCCI are different than those observed for SACI. Additionally, it was demonstrated that the amount of heat released in a given cycle can be predicted, based on previous combustion cycles. Larimore et al. [30] investigated SACI at stoichiometric conditions and argued that the fuel from an incomplete combustion cycle interferes with combustion in a couple of following cycles until it is completely burnt. Thus, the mechanism responsible for CCV in SACI is similar to the one observed in conventional HCCI by Hellström et al. [12] or Koopmans et al. [16]. Moreover, in SACI, residual fuel appears to increase the HRR of the flame propagation phase.

To facilitate recognition between flame propagation and kinetic combustion Ortiz-Soto et al. [31] proposed a method to identify the auto-ignition set point in SACI. The procedure utilised analysis of the HRR´s second derivative. Chang et al. [32] used this procedure to estimate fractions of fuel consumed by flame propagation. The research was performed with NVO, at 2000 rpm and for stoichiometric conditions. At spark advance (SA) of 34 CAD before top dead centre (TDC) and at ambient intake temperature, the flame propagation fraction was estimated at 28% of the total fuel energy. While increasing the intake

temperature this fraction reduced in favour of the kinetic phase. In research by Zhou et al. [33], performed under similar conditions, 20% of the total fuel mass was burnt by flame propagation. The fraction of fuel burnt from the spark discharge was insensitive to SA, whereas it was substantially affected by NVO-driven I-EGR.

Yıldız and Albayrak Çeper [34] preheated intake-air to support auto-ignition in SACI and, similarly to Ortiz-Soto et al. [31], used HRR´s second derivative to identify transition from SI to HCCI combustion. The authors however, focused on analysing this transition on the individual cycle basis. They found that there is a good agreement between the start of kinetic combustion and 10% mass fraction burnt (MFB). However, the flame propagation duration was not correlated with the estimated amount of fuel burnt in this mode.

In summary, low-temperature HCCI combustion provides superior efficiency with ultra-low NO_X emissions, but the concept needs to work either as part of hybrid propulsion and/or switch to conventional SI mode for real-world application. Either way, extending the high-load limit of low-temperature operation remains a particular challenge. Spark assist offers potential for high-load HCCI extension by managing the cycle-specific pressure rise rate (PRR) and combustion variability to give more controllable combustion.

On one hand, the SACI concept is relatively mature and automotive industry front-runners are already introducing market-ready solutions [35], [36], with in-cylinder pressure-based control considered an enabler [37]. On the other hand, the primary focus of most university-level works is understanding the mechanisms of SACI combustion, particularly combustion variability [38], [30]. The high-level vision of the governing mechanisms is fairly unified across individual research groups, but on the detail level, however, inconsistencies are reported in the behaviour of individual combustion indicators from cycle to cycle [39].

Importantly, most of those works, despite providing valuable contribution to the fundamentals of SACI, lack the proper applicable context. Considering the current boundary of SACI technology, further research in this area should focus on building the fundamental knowledge of this combustion to take it towards its possible application in engine control.

Considering the above shortcomings in the state of the art, we have set the following objectives for the present work:

1. Demonstrate the feasibility of HCCI´s high-load operation with spark assist, taking into account relevant constraints for contemporary automotive applications.
2. Validate new, faster methods for in-cycle combustion analysis for SACI-specific phenomena.

3. With improved methods, deepen the insight into the mechanisms enabling load extension in SACI.
4. Use the extended insight into SACI´s cyclic performance to seek correlations between characteristic combustion determinants, paving the way for improved control measures in SACI.

Achieving objective 1 gives the proper context for the remaining three objectives. Objectives 2 and 3 serve the current needs of fundamental level research: objective 4 shifts the focus towards real-world applications.

To realize the objectives, the present research combines single-cylinder research engine tests with high fidelity combustion analysis performed on an individual cycle basis. The tests are focused on boundary conditions of high-load NVO-HCCI (1500 rpm, and around 0.5 MPa IMEP), realised through two different mixture strategies: stoichiometric and lean combustion with high I-EGR dilution. Both strategies are feasible in terms of their applicability, but constrained in different aspects. The SACI test matrix comprised a SA sweep performed for each of the two mixture´s representative operating points. The experimental framework is comprehensively discussed in Section 2. Note that, because of a very technical nature of the research questions answered by this work, we specify them gradually through the course of the results discussion (Section 3), instead of naming them at this point. For the readers convenience the research questions are then listed, and explicitly answered, in the wrapping up discussion (Section 4) before jumping into objective-oriented conclusions in Section 5.

2. Methods

2.1. The experimental setup

A single-cylinder research engine with a displacement of 0.5 dm^3 and compression ratio of 11.7:1 was used in this research. Its bowl-shaped combustion chamber was located in the engine head. The piston crown was flat but included a small squish-generating rim for improved in-cylinder mixing of fuel. Direct fuel injection was via a side-mounted, swirl-type, single-stream Bosch HDEV electromagnetic injector. The injector was positioned tangentially to the intake port and inclined by 38 degrees from the cylinder axis. The engine was equipped with variable valve actuation with hydraulically controlled valve lift to achieve HCCI combustion using NVO [40]. Table 1 provides the specification of the research engine.

The engine test stand was equipped with a direct current dynamometer and precise thermal conditioning system for the intake air, cooling liquid and lubricating oil, facilitating a setpoint temperature with a single degree accuracy. The duration and timing of fuel injection, as well as spark timing, were controlled with a PC-based system using dedicated in-house software.

The engine test stand was also equipped with all necessary sensors and both the low- and high-frequency signals were managed by a data acquisition system. An AVL GH12D miniature pressure transducer installed directly in the engine head recorded in-cylinder pressure, with a resolution of 0.1 CAD. Exhaust gas composition was measured with an AVL Fourier transform infrared (FTIR) analytical system. The excess air ratio (λ) was measured with a Bosch LSU 4.2 oxygen sensor, with an ETAS LA4 lambda meter also used for verification. The system also included an AVL fuel balance, an intake-air mass-flow meter and a set of pressure and temperature transducers for measuring intake and exhaust thermodynamic conditions.

Table 1. Research engine specifications.

Parameter	**Value**
Displacement	498.5 cm^3
Bore	84 mm
Stroke	90 mm
Compression ratio	11.7:1
No. of valves	2
Fuel injector	Direct, side-mounted, single-hole, swirl-type
Air-path	Naturally aspirated

2.2. Experimental conditions and procedure

The engine speed was held constant at 1500 rpm for all the tests. The engine was fuelled with commercial gasoline with a research octane number of 95. The valvetrain was set to NVO mode with symmetrical timings of exhaust valve closing and intake valve opening to give an NVO period of 160 CAD. The valve lift profiles, example engine pressure cycle developed by the engine and example electrical command signal traces are shown in Fig. 1. Note that all CA domain values quoted in this paper are after TDC at NVO event. For clarity, the SA quoted is the distance between the spark event and TDC in the main event. Fuel was

injected directly into the cylinder at the end of NVO expansion. The start of injection (SOI) was maintained constant at 60 CAD and injection was completed before intake valve opening. This injection strategy allowed mixture homogeneity in the main cycle, whereas fuel reforming (chemical reactions between fuel and recompressed exhaust gases) was avoided by injecting during the cold part of the NVO cycle. This disables the feedback loop in terms of NVO chemical phenomena, which would contribute to additional cycle-to-cycle variability. The effects of NVO fuel/exhaust processes were analysed in detail in [41], while works [21] and [42] analysed these phenomena also in terms of cycle-to-cycle variability.

The experiment explored combustion evolution of dual-mode HCCI-SACI engine operation. To this end, the engine was operated as autonomous HCCI (without spark discharge) and as SACI with variable SA. This parameter was swept from the point when the spark discharge was set at TDC firing (SA = 0 CAD) and advanced as early as possible, until the CA50 reached TDC. Two mixture conditions were explored: a stoichiometric mixture and a slightly lean mixture (λ = 1.1). Different fuel values were injected (approximately 15.3 mg/cycle and 12 mg/cycle respectively) to achieve these two mixture strengths, with atmospheric manifold absolute pressure (MAP). This provided net IMEP levels of 0.53 MPa and 0.42 MPa for the stoichiometric and the lean case respectively.

These two mixture strengths mimicked the operating conditions when NVO-HCCI operation reaches its high-load limit due to insufficient air aspiration. This approach enables us to assess how spark assist can extend the high-load operation limit of HCCI by reducing its CCV near the transition region towards conventional SI operation.

Although the two investigated operating points are close to each other with respect to their excess air ratios (λ), they differ considerably in terms of overall fuel dilution. This is associated to the inbound NVO effect of mixture strength on the amount of internally recirculated exhaust. To quantify the cumulative effect of intake air and I-EGR on total fuel dilution, a fuel-charge equivalence ratio is defined as follows:

$$\Phi = \frac{m_F}{m_A + m_{\mathrm{EGR}}} \left(\frac{m_A}{m_F}\right)_{stoi}, \quad (1)$$

where m_F is mass of fuel, m_A – mass of air, m_{EGR} is mass of recirculated exhaust and $\left(\frac{m_A}{m_F}\right)_{stoi}$ is stoichiometric air requirement of fuel. Using this metric, the effect of the applied λ change from 1 to 1.1 translates to Φ from 0.6 to 0.45 accordingly. The two selected mixture composition levels are referred as stoichiometric and lean operation throughout this study. Table 2 lists the engine and combustion control parameters. Additionally, it should be noted

that λ was a controlled value and was maintained by corrections of injected fuel, so IMEP and fuel dilution were not explicitly controlled.

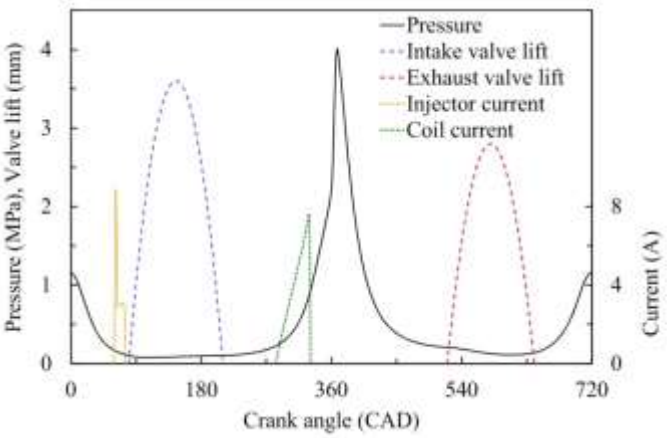

Fig. 1. Example in-cylinder pressure, calculated valve lifts and injection and ignition current commands as a function of crank angle.

Table 2. Engine operation parameters.

Parameter name	Value	
Engine speed	1500 rpm	
SOI	60 CAD	
MAP	100 kPa	
Coolant temperature	90 °C	
Intake air temperature	30 °C	
Fuel rail pressure	10 MPa	
Condition name	**Stoichiometric**	**Lean**
Mass of fuel	~15.3 mg/cycle	~12 mg/cycle
λ	1.0	1.1
Mass of recirculated exhaust	~152 mg/cycle	~190 mg/cycle
Φ	~0.6	~0.45
Net IMEP	~0.53 MPa	~0.42 MPa

2.3. Data analysis

2.3.1 In-cylinder pressure analysis

In-cylinder pressure is instrumental for the study´s detail data analysis. The recorded relative pressure traces for individual cycles were filtered and pegged to provide accuracy of

the pressure-derived values. To this end, the absolute pressure signal from the intake port was used as a reference value to correct in-cylinder pressure around the point where valve flow was stopped. Note that thermodynamic analysis of in-cylinder pressure was supported by a 0-dimentional flow model. The pegging procedure was applied to each separate engine cycle.

PRR and IMEP were calculated directly from in-cylinder pressure. Each was calculated separately for 1000 cycles and then averaged. Indicated specific fuel consumption (ISFC) and indicated specific emissions were determined on the basis of average IMEP.

Analysis of the in-cylinder pressure cycles (on the cycle-to-cycle basis) was based on the first law of thermodynamics. The apparent heat release rate was calculated using the following formula:

$$\mathrm{HRR} = \frac{\gamma}{\gamma-1} p \cdot \Delta V + \frac{1}{\gamma-1} V \cdot \Delta p \tag{2}$$

where the discrete derivatives of volume (ΔV) and pressure (Δp) were calculated every 0.1 CAD. The ratio of specific heats (γ) was calculated from the instantaneous temperature and composition of the in-cylinder mixture. Note, that a similar procedure has been thoroughly described by Lapuerta et al. [43]. The bulk gas temperature was calculated at every CA, using the equation of state with consideration of the effect of mixture composition on the gas constant. With the instantaneous gas temperature calculated, the cylinder heat loss was modelled using the Hohenberg correlation for heat transfer coefficient [44]. The cumulative gross heat release (CHR), obtained by numerical integration of HRR from Eq. 2 corrected with the heat-loss model, served as the basis for calculating the crank angle of 5%, 50% and 95% of the cumulative heat release. These combustion indicators are denoted as CA05, CA50 and CA95 respectively, and are graphically explained in Fig. 2. Combustion durations are defined as differences between combustion progress indicators. For instance, CA05-95 denotes the combustion duration between CA05 and CA95. The intermediate combustion durations CA05-50 and CA50-95 are also used in this work, as depicted in Fig. 3. These indicators are calculated on the individual cycle basis.

Several indicators are used to address CCV. Conventionally, CCV is addressed by coefficient of variation (CoV) in IMEP. This includes the effects of variability in fuelling and thermal efficiency, which is a superposition of the following main components: combustion efficiency, combustion timing and heat transfer. In order to decouple the variability in timing, standard deviations of CA05, CA50 and combustion durations are analysed. Additionally, several parameters are analysed on an individual cycle basis to support understanding of the phenomena. Accordingly, cycle specific CA50 and CA95 are further used to determine the

start of the kinetic phase in subsequent cycles. The methodological background for this determination is introduced in the following subsections 2.3.1 and 2.3.2.

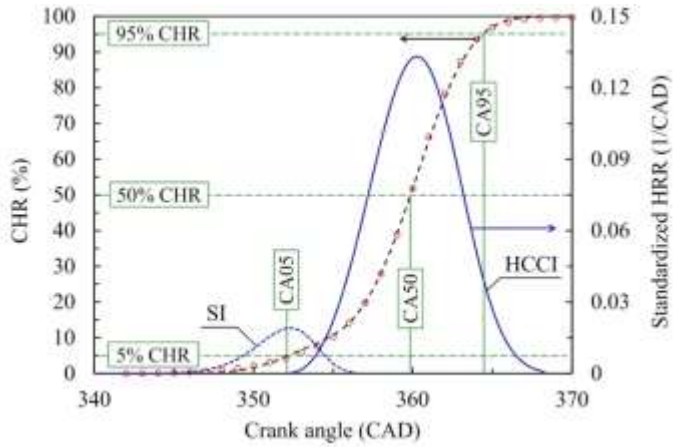

Fig. 2. Exemplary experimental standardized CHR (o) with marked combustion indicator definitions. The black line (--) denotes the CHR fit using the double Wiebe model. The blue lines represent the resulting Wiebe HRR functions corresponding to the fractions of fuel burned by flame propagation (SI) and kinetic combustion (HCCI).

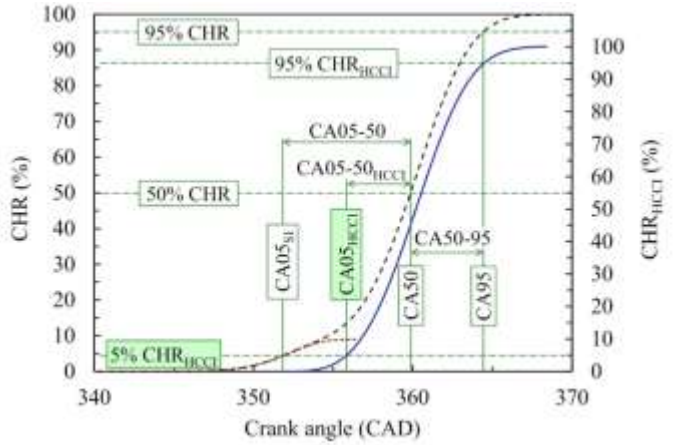

Fig. 3. Modelled CHR (--) as a spline of SI-dominant flame propagation (..) and HCCI-like kinetic combustion (-). Additional marked specific combustion indicators characterise individual combustion modes $CA05_{SI}$ and $CA05_{HCCI}$. Same case as Fig. 2.

2.3.2 Determining the energy split between flame propagation and kinetic combustion

A numerical procedure was developed to facilitate recognition between flame propagation and kinetic combustion. A double Wiebe spline function, capable of reproducing two-stage combustion was used [45]. Fitting of the double Wiebe model to experimental CHR curves

incorporated the successive approximation method and identified seven parameters, as specified in Eq. 3.

$$\mathrm{CHR}_{\mathrm{Wiebe}} = x_{\mathrm{SI}}\left(1 - e^{-6.908 {y_{\mathrm{SI}}}^{m_{\mathrm{SI}}}}\right) + x_{\mathrm{HCCI}}\left(1 - e^{-6.908 {y_{\mathrm{HCCI}}}^{m_{\mathrm{HCCI}}}}\right). \quad (3)$$

Parameters x_{SI} and x_{HCCI} can be interpreted as fractions of the fuel burnt through flame propagation and kinetic combustion respectively. Note that $x_{\mathrm{SI}} + x_{\mathrm{HCCI}} = 1$. The exponents m, with the same indices, are Wiebe function shape parameters, whereas y_{SI} and y_{HCCI} represent the progress of each mode of combustion, calculated as follows

$$y = \frac{\alpha - \mathrm{SOC}}{\mathrm{EOC} - \mathrm{SOC}}. \quad (4)$$

In Eq. 4 α is the instantaneous CA and SOC and EOC denote CAs of start and end of combustion respectively. The reader is referred to Heywood's Internal Combustion Engine Fundamentals for more details on the Wiebe combustion model and its application [46]. Note that the conventional way to apportion MFB to determine energy split between flame propagation and kinetic combustion is to use the HRR second derivative [32], [33]. Finally, it should be noted that due to calculation time limitations, this procedure was applied for cycle-averaged pressure traces.

2.3.3. Proprietary method for designating start of kinetic combustion, based on standard combustion indicators

Figure 2 shows the results of fitting the double Wiebe model in Eq. 3 to the experimental CHR, along with individual derivatives (HRRs) corresponding to the fractions of fuel burnt by flame propagation (SI) and kinetic combustion (HCCI). Figure 3 presents the same combustion mode split based on cumulative values of individual heat release rates. By structure of Eq. 3, the total combustion duration is a sum of flame propagation (SI) and kinetic (HCCI) combustion. If we take the spark (SP) event as the overall SOC and CA95 as the global EOC, additionally simplifying the $\mathrm{CA95}_{\mathrm{HCCI}}$ and global CA95 overlap, the above statement takes the form:

$$\mathrm{CASP{-}95} = \mathrm{CASP{-}95}_{\mathrm{SI}} + \mathrm{CA05{-}95}_{\mathrm{HCCI}}. \quad (5)$$

Regarding the SACI combustion phenomena, most research [31], [47] consistently indicates that the start of kinetic combustion (denoted as $\mathrm{CA05}_{\mathrm{HCCI}}$) appears just after the flame propagation is completed, as demonstrated in Fig.3. Thus, the flame propagation duration in Eq. 5, can be estimated as:

$$\mathrm{CASP{-}95}_{\mathrm{SI}} \approx \mathrm{CA05}_{\mathrm{HCCI}} - \mathrm{CASP}. \quad (6)$$

From Fig. 3, one can further note that starting from CA50, the global combustion progress (black dashed line) is fully governed by kinetic combustion (blue line), which is almost linear until the global CA95. Hence, the kinetic combustion can be estimated as:

$$\mathrm{CA05{-}95_{HCCI}} \approx 2 \cdot \mathrm{CA50{-}95}. \quad (7)$$

Merging the above approximations of the flame propagation duration (Eq. 6) and kinetic combustion duration (Eq. 7) yields:

$$\mathrm{CA05_{HCCI}} \approx 2 \cdot \mathrm{CA50} - \mathrm{CA95}. \quad (8)$$

As indicated above, $CA05_{HCCI}$ can be considered as the transition point between flame propagation and kinetic combustion in SACI. Eq. 8 provides a method to estimate this point through commonly used combustion indicators, real-time calculable with the standard heat release analysis governed by Eq. 2.

The above method is used on the cycle-to-cycle basis to provide the insight to the origin of CCV in the present paper. This insight further relies on the estimation of the temperature rise (ΔT_{SP}) due to flame propagation. This indicator is calculated as the difference between the polytropic compression temperature and the bulk in-cylinder temperature from the equation of state. The polytropic exponent is estimated by matching the polytropic model to the measured in-cylinder pressure before the spark discharge.

3. Results

3.1. CCV and PRR dilemma for HCCI load extension

Figure 4 gives an insight into combustion characteristics within the constraints of the discussed operating modes. It provides in-cylinder pressure traces averaged over 1000 consecutive cycles. It is evident that in SACI, the earlier the spark the earlier the combustion commences and hence the higher the peak pressure. As the spark event approaches TDC (SA approaching zero), the combustion characteristics move closer towards those of autonomous HCCI. For the lean concept ($\Phi = 0.45$) this happens already around SA = 10 CAD TDC, when on the averaged basis, auto-ignition commences before any relevant fuel is burned through spark discharge.

Moving closer to full stoichiometry and Φ of 0.6 (refer to Fig. 4b) enables easier ignition of the fuel mixture, both in the autonomous and spark assisted cases. In the respective SA setpoints combustion starts earlier compared to the lean case and is attributed to significantly elevated peak pressure and pressure rise rate (PRR).

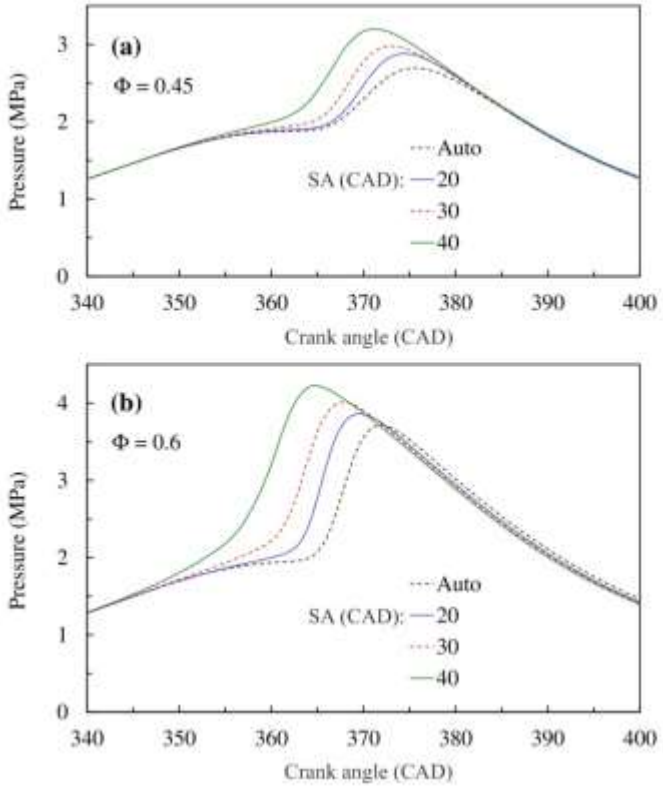

Fig. 4. Cycle averaged in-cylinder pressure curves; a) Φ = 0.45 b) Φ = 0.6.

For low temperature combustion (LTC) concepts in particular, excessive PRR forms an important constraint because it usually limits the ability to reach high load operation before peak pressure [48]. The PRR is limited by engine durability and combustion noise issues, dictating a typical borderline range of 0.6-0.7 MPa/CAD [34]. On the other hand, combustion is considered stable if CoV in IMEP does not exceed 4% [49]. Figure 5 illustrates how the discussed combustion concepts perform with respect to PRR and assesses this performance against the CoV in IMEP stability criterion.

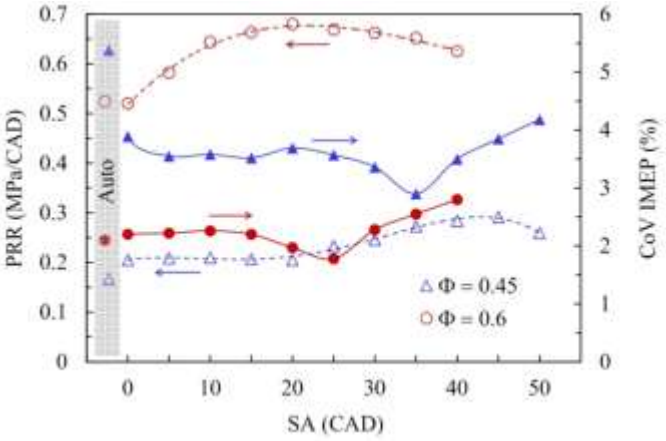

Fig. 5. Pressure rise rates and CoV in IMEP versus spark advance for all investigated conditions. Shaded area indicates results for autonomous operation.

For the lean case (blue points in Fig. 5), autonomous HCCI results in high combustion variations (CoV in IMEP = 5.4 %) and yet has acceptable PRR. Adding the spark discharge elavates the PRR slightly, yet provides considerable reduction in CoV in IMEP, with potential to bring the variations below the 4% stability benchmark. At stochimetric conditions (red points in Fig. 5), HCCI is already within the acceptable combustion variation limit, but PRR is very high. Introducing spark assist moves PRR very close to the 0.7 MPa/CAD limit but does not provide further reduction in combustion variations in terms of CoV in IMEP. Interestingly, the CoV in IMEP exhibits a highly non-monotonic trend with respect to SA for both mixture conditions. This implies the existence of a local minima in CCV at any particular (mixture conditions-dependent) SA setpoint.

Figure 6 depicts ISFC and NO_X emissions, completing the picture of the relevant constraints for the considered HCCI and SACI concepts. Emissions and performance are not the principle focus of the present discussion, so analysis of Fig. 6 is brief. For a detailed benchmark assessment of HCCI and SACI in terms of those indicators, one is referred to Hunicz et al. [48].

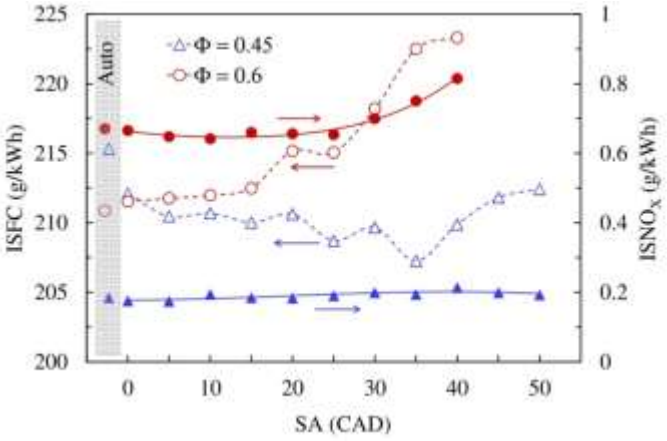

Fig. 6. Indicated specific fuel consumption and NO_X emissions versus spark advance for all investigated conditions. Shaded area indicates results for autonomous operation.

Note that the qualitative difference between HCCI at lean and stoichiometric conditions lies in NO_X emissions. The lean case provides over 70% reduction in engine-out NO_X emissions compared to HCCI with stoichiometric strategy. The lean case´s high fuel dilution reduces combustion temperature, explaining its ability to reach ultra-low (0.2 g/kWh) engine-out NO_X emissions. That is half the NO_X limit (brake specific) set by the current Euro-VI heavy duty emission standards. Spark assist does not introduce a major sensitivity to NO_X.

The baseline HCCI-stoichiometric strategy has, however, around 2% lower fuel consumption than the lean case (Fig. 6). Note that the lean case´s fuel consumption is heavily correlated with CoV in IMEP, and introducing spark assist reduces its ISFC to the level of the stoichiometric case, crucially, without jeopardizing NO_X emissions. Note that the local minimum of CoV in IMEP, observed for the lean case at SA = 35 CAD (Fig. 5), coincides with the minimum ISFC. Thus, keeping CCV low has a profound effect on engine efficiency during HCCI/SACI operation. Note that advancing the SA worsens ISFC for the stoichiometric case. The main cause of this deterioration is combustion being phased too early, as seen in Fig. 4b. Still, the effect of reduced CoV in IMEP is visible in the inflection point of the ISFC trend line at SA = 25 CAD (Fig. 6). Compare the stoichiometric case in Figs. 5 and 6 for details.

The main takeaway from this section is that both mixture conditions give feasible high-load transition points from HCCI through SACI to conventional SI operation. It is desirable to extend the load range of the HCCI/SACI mode to improve both efficiency and emissions. HCCI load range is limited by combustion stability at lean conditions, while at stoichiometric operation the transition is forced mainly by excessive PRR. At lean conditions, SACI can

provide bigger improvement potential in CCV reduction, coupled with a superior efficiency and NO_X trade-off.

3.2. Heat release analysis and combustion timings

Figure 7 shows the results of cycle-averaged gross HRRs (Eq. 2 corected on heat loss) for the HCCI and SACI cases presented in Fig. 4. Note that for the lean case in Fig. 7a, SACI causes more rapid combustion compared to the autonomous HCCI case. Advancing the SA does not increase the peak HRR value and the associated increase in PRR, observed in Fig. 5. This mainly is due to the superposition of roughly constant combustion progress with earlier combustion phasing (reducing the expansion-driven pressure drop). Although the lean case´s peak HRRs and overall combustion durations are broadly unchanged while increasing the SA, the contribution of flame propagation starts to become more pronounced. This manifests in a reduced slope of the HRR curve in the initial phases of the combustion (compare HRRs for diferent SA in Fig. 7a). The mechanism is reinforced for the stoichiometric case, as the HRR for SA = 40 CAD in Fig. 7b exhibits a clear inflection point around 355 CAD, indicating the start of the kinetic phase of combustion.

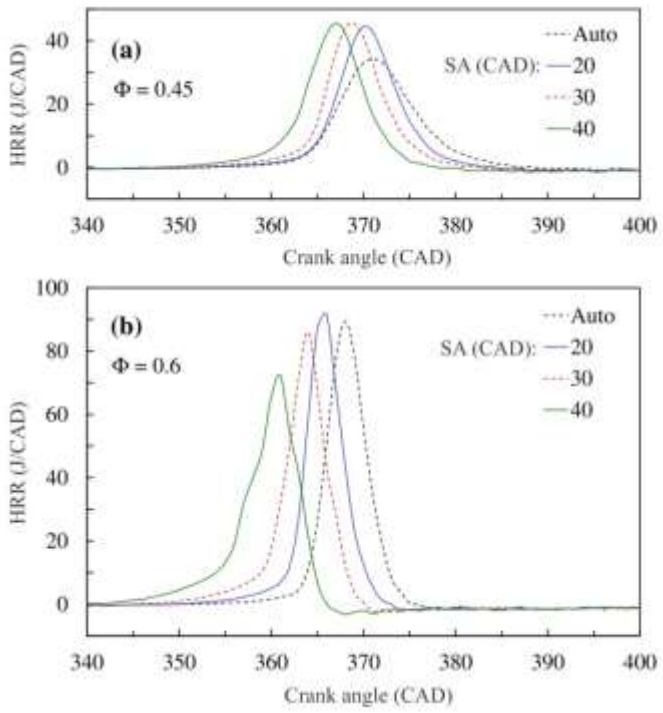

Fig. 7. Cycle-averaged calculated gross HRR curves; a) Φ = 0.45 b) Φ = 0.6.

Figures 8 to 10 synergize the information carried by heat release rates (Fig. 7) into combustion phasing (CA05, CA50) and combustion duration (CA05-50). This facilitates further discussion on cycle-to-cycle combustion parameters at different SAs. The parameters are calculated separately for 1000 consecutive cycles, and then averaged. Standard deviation (STD) is used to quantify CCV.

Figure 8 shows the results of CA50 for HCCI and SACI with different spark timings. CA50 is an important parameter since it is bounded by the constraints discussed in Section 3.1. Namely, CA50 should be maintained between 365 CAD and 370 CAD in order to optimise how the pressure rise is put into useful work. Timing later than 370 CAD penalises indicated efficiency due to pressure rise being hindered by the expansion. CA50 earlier than 365 CAD causes excessive pressure-rise rates and puts the early phases of combustion before TDC, contributing to negative work. Note that phasing that is too early is predominantly responsible for the rapid increase in ISFC for the stoichiometric case with SA above 20 CAD (reflected in Figs. 6 and 8 results).

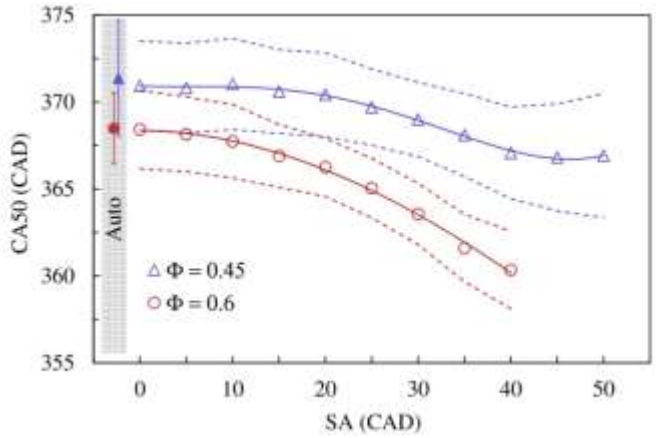

Fig. 8. CA50 values averaged over 1000 consecutive cycles versus spark advance for all investigated conditions. Filled points show autonomous operation. Error bars and dashed lines show STDs at respective points.

Figure 8 shows that applying spark discharge close to TDC has no significant effect on CA50 when compared to autonomous operation. Moreover, in the case of lean mixture, the effect of ignition on the CA50 remains almost imperceptible even when the ignition is advanced by 10 CAD. Further advancing the spark discharge advances combustion for all conditions, but the spark effect differs, depending on mixture strength. At lean conditions, the difference in CA50 between autonomous operation and SA = 40 CAD is approximately

4 CAD. For stoichiometric conditions, this difference is more than doubled. This confirms the observations derived from Fig. 7 and implies that the stoichiometric case is more prone to support development of a propagating flame that accelerates kinetic combustion.

Another interesting observation derived from Fig. 8 is that there is a very good agreement between STDs of CA50 (error bars and dotted lines) and CCV expressed by CoV in IMEP (Fig. 5). Both phenomena, namely the sensitivity of CA50 when switching from mode to mode, and further sensitivity of STD CA50 to SA timing, will be addressed more specifically in Section 3.3.

Figure 9 shows trends in CA05. This is the early stage of combustion and therefore should be more sensitive to flame development than CA50. However, a comparison of Figs. 8 and 9 reveals that the dynamics of both combustion timing indicators are similar, especially for the lean mixture. This can be explained by the relatively small amounts of heat released during flame propagation attributed to the current research. Subsection 3.4 provides more insight into this issue. It is sufficient to mention that for stoichiometric mixture and SA = 40 CAD, the share of heat released by flame propagation is only 9%. Obviously, the leaner the mixture and the later the spark, the lower the SI combustion fraction.

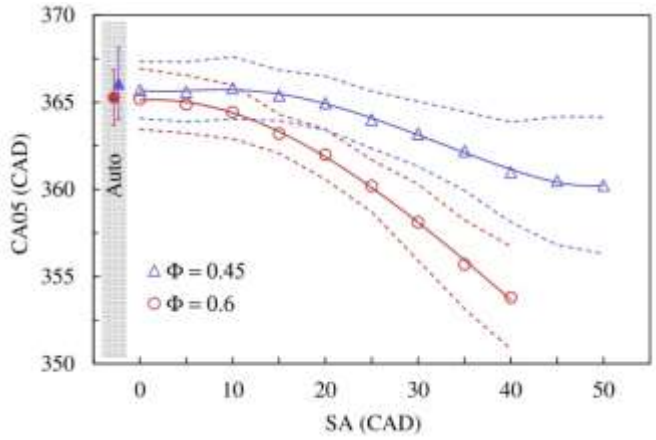

Fig. 9. Mean values of CA05 versus spark advance for all investigated conditions. Filled points show autonomous operation. Error bars and dashed lines show STDs at respective points.

Interestingly, in both cases the STD of CA05 is the smallest for SA at approximately 20 CAD. This indicates that flame development in these conditions is the most stable. It is a superposition of two factors. First, mixture density is high enough to enable fast and stable flame development. Second, the flame propagation fraction is small and immediately

followed by kinetic combustion. As a result, CA05 is identified at the stage where HRR increases rapidly.

Figure 10 completes the discussion of the individual timing indicators CA05 and CA50, addressing how they tend to change with respect to each other. For SA below 10 CAD the combustion duration remains unchanged because both CA05 and CA50 are affected in exactly the same way (compare Figs. 8, 9 and 10). Further increasing the SA has a pronounced effect on combustion duration, especially for the stoichiometric case, for which the CA05-50 increases linearly by approximately 1.1 CAD per 10 CAD increment in SA. For the lean case, the stagnation is broken at 5 CAD greater SA, and then the combustion duration increases linearly from this point, but with a much lower gradient of 0.4 CAD per 10 CAD of SA. Note that for autonomous operation and late spark ignitions, combustion of the stoichiometric mixture is much quicker than the lean mixture´s. CA05-50 durations become the same for lean and stoichiometric mixtures at advanced spark timings.

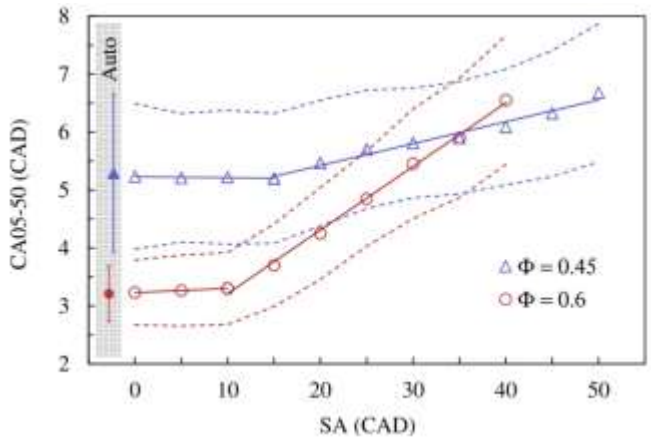

Fig. 10. Mean values of CA05-50 versus spark advance for all investigated conditions. Filled points show autonomous operation. Error bars and dashed lines show STDs at respective points.

STDs of CA05-50 differ for the two investigated mixture strengths. For the stoichiometric mixture, SA increases variability linearly, from 0.5 CAD to 1.1 CAD. For the lean mixture, SA has a non-monotonic effect: advancing the spark from TDC to 30 CAD reduces CA05-50 variability, while further advance increases it. The behaviour of STD(CA05-50) contrasts with the results of STD of the individual timing parameters that comprise CA05-50, adding to the overall pool of phenomena that need a deeper understanding. The following sections

contribute to this insight and the final discussion of CCV phenomena is provided in Section 3.6.

3.3. Correlating combustion timing indicators on the individual cycle basis

The effects of spark assistance on the early and late stages of combustion can be understood when we correlate CA05-50 against CA50-95 on an individual cycle basis. Figure 11 presents the results of this correlation for 1000 consecutive cycles of autonomous and spark-assisted operation.

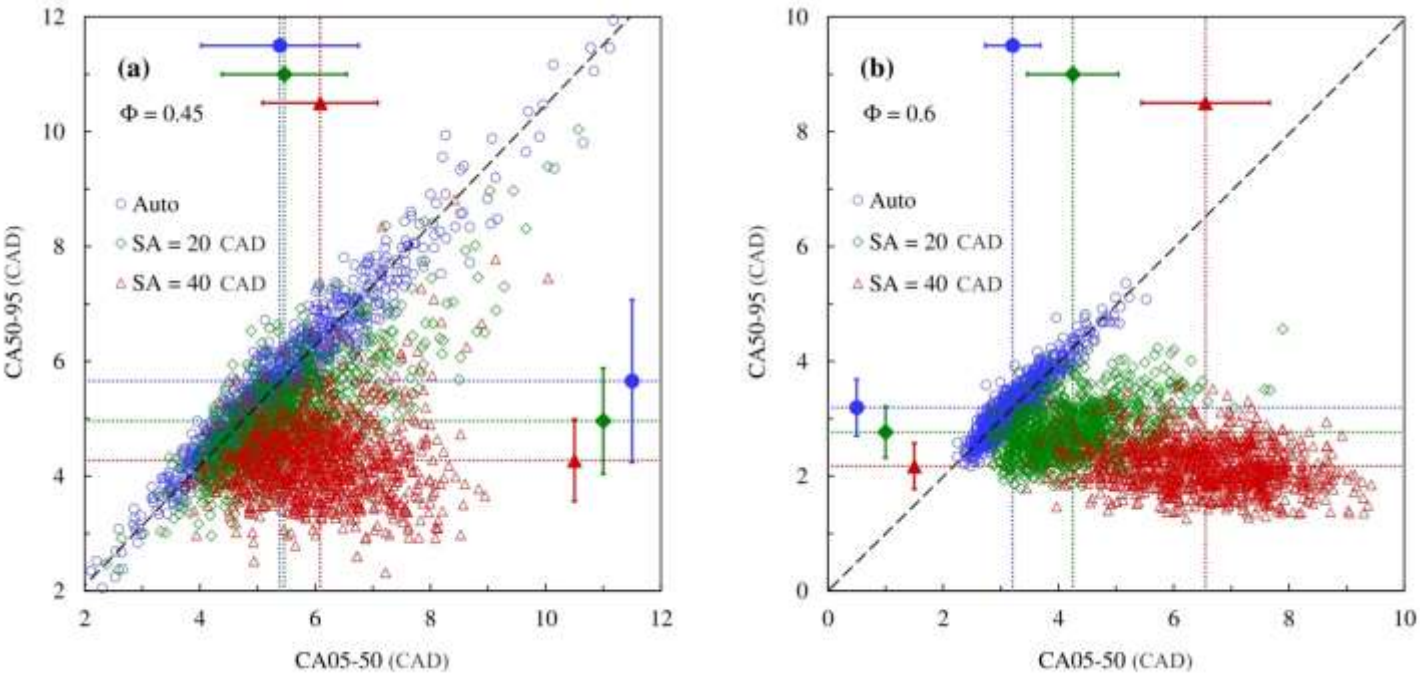

Fig. 11. CA50-95 versus CA05-50 for autonomous HCCI and SACI; a) Φ = 0.45, b) Φ = 0.6. Black dotted line presents a linear fit for autonomous HCCI. Filled points and error bars show mean values and STDs respectively.

Immediately apparent from Fig. 11 is a close correlation between the early and late stages of combustion for autonomous HCCI (blue points). For the stoichiometric case these parameters are corralled close to 1 to 1. For the lean case, the deviation from unity is minor. We will come back to this issue at the latter part of the discussion.

At this point, it is important to notice that under spark-assisted operation at SA = 20 CAD, the distribution of CA05-50 vs CA50-95 depends heavily on mixture strengths. Under lean conditions, spark assist does not affect the majority of cycles, which concentrate near the

regression line. There are also cycles far below the line. For such cycles, a fast CA50-95 period appears after a relatively long CA05-50 period. This indicates strong flame propagation, which increases pressure and temperature during the initial combustion phase, thus raising the reaction rate during the kinetic phase. For the stoichiometric SACI at SA = 20 CAD, the majority of cycles reveal asymmetry, with evident fraction of flame propagation. For SA = 40 CAD there is literally no correlation between CA05-50 and CA50-95, neither for stoichiometric nor lean cases. The above observations suggest that the first stage of combustion is controlled by flame propagation, whereas the second stage is controlled by chemical kinetics.

This reasoning is proven by strong correlation of CA50-95 and in-cylinder temperature, calculated for CA location where peak pressure appears. This is depicted for both mixture strengths in Fig. 12. A comparison of the two graphs in Fig. 12 reveals that corresponding points for both mixture strengths lay on the same trend line. This is a reasonable outcome because HCCI kinetic combustion rate is determined by temperature rather than by fuel concentration [50].

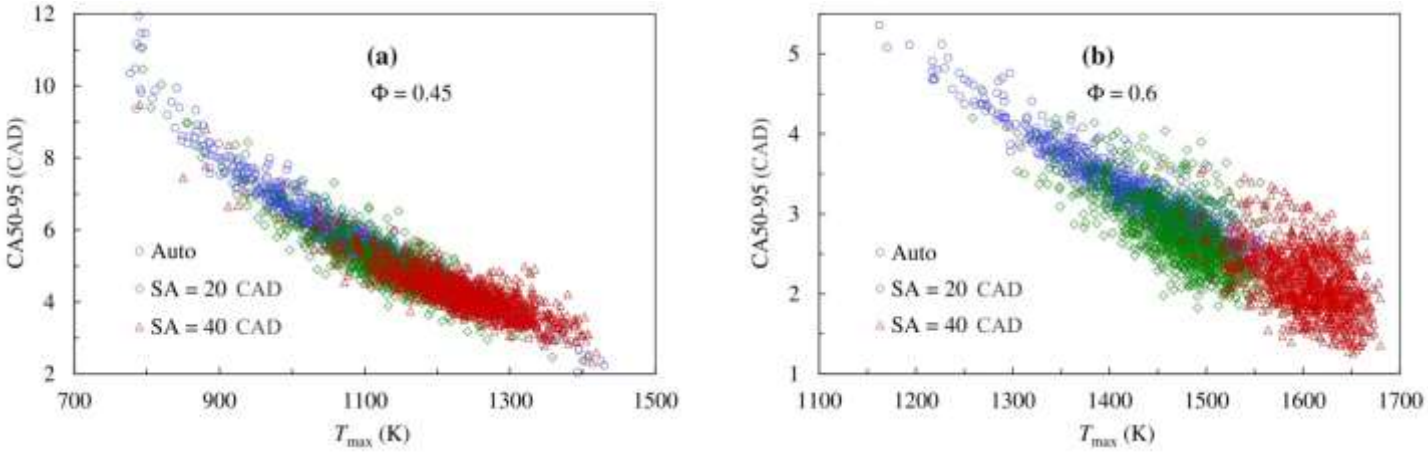

Fig. 12. CA50-95 versus in-cylinder temperature at peak pressure for autonomous HCCI and SACI operation; a) Φ = 0.45, b) Φ = 0.6.

The points creating a vertical line on the left of Fig. 12a are formed by temperature at TDC. They represent very late cycles for which the maximum combustion pressure was lower than the pressure resulting solely from compression. Obviously, such cycles are most typical of autonomous HCCI and late SA, where the spark effect on combustion is lower. There are no very late cycles for the stoichiometric mixture.

It is important to return to the issue of symmetry between CA05-50 and CA50-95 for autonomous HCCI operation, raised in Fig. 11. It is examined more closely at the end of this section. Its importance is derived from the fact that the assumption about this symmetry is crucial for the method applied in section 3.4 to separate flame propagation and kinetic combustion. Section 2.3.2. provides details of the method itself.

Note, that for the stoichiometric HCCI, the symmetry between CA05-50 and CA50-95 is evident in Fig. 11b. For the lean case, the slight deviation from direct symmetry observed in Fig. 11a is apparent and comes from the adopted calculation methodology of combustion timing indicators. This is based on gross CHR, which does not take the unburned hydrocarbons into account, resulting in overestimation of CA95 for cases with low combustion efficiency. With large CCV attributed to the lean autonomous case, elongated combustion cycles (visible on the far right of Fig. 11a) are ultimately the ones with poor combustion efficiency, hence the apparent deviation from symmetry between CA05-95 and CA50-95. The CHR curve itself, therefore, can be symmetrical for HCCI in both mixture conditions.

3.4. Fractionating flame propagation and kinetic combustion

The above discussion revealed complex effects of spark assistance on combustion timing, but with only qualitative assessment of flame propagation. In order to quantify the energy split between flame propagation and kinetic combustion, the double Wiebe function (Eq. 3) is fitted to the experimental CHR. Figure 13 presents the fraction of the heat released during the flame propagation period (x_{SI}). Note that x_{SI} values are calculated for ensemble-averaged CHR curves.

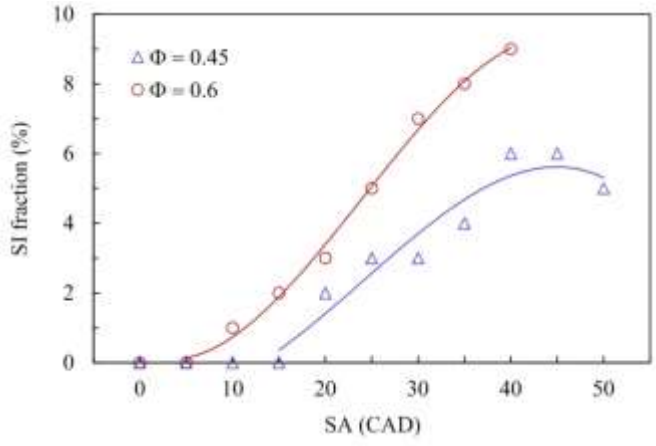

Fig. 13. Calculated fraction of heat released in SI mode for all investigated conditions.

Figure 13 indicates that for the lean mixture, the flame propagation was not detected by first law analysis for SA less than 20 CAD. Further advancement of the spark gradually increased the amount of heat released in SI mode, reaching a maximum of 6% at SA = 40 CAD. Some stagnation or even reduction in SI fraction can be noted beyond this point. Such a result is reasonable because, at diluted mixtures and under low-pressure conditions, flame propagation is slow and vulnerable to quenching by the heat flow to the unburnt zone. Turning to the stoichiometric mixture, noticeable flame propagation starts with less spark advance, at 10 CAD. Also, due to lower fuel dilution, flame propagation increases the amount of heat released in the SI mode more rapidly, before auto-ignition appears. Comparison of Figs. 9 and 13 reveals good agreement between CA05 and SI fraction.

It is worth noticing that the SI fractions reported in Fig. 13 are generally quite small compared to those from other SACI research. For instance, the fractions obtained in the studies by Chang et al. [32] and Zhou et al. [33] were at least twice as high. Note that the mentioned research used experimental platforms that were similar to each other and explored similar mixture conditions. The differences can be attributed to our engine´s side-mounted spark plug. This combustion chamber configuration provides slower flame propagation than one with a centrally located spark plug, which was the case for the referred research.

The energy fractions calculated for cycle-averaged data, commonly used in previous works committed to understanding SACI combustion [32], [33], do not provide the necessary insight to the phenomena in individual cycles. In Section 2.3.3, we introduced an alternative approach to quantify the intensity of flame propagation and kinetic combustion. This method senses the start of kinetic combustion ($CA05_{HCCI}$) based on conventional HRR analysis and, contrary to the commonly used Wiebe approach, is real-time capable. Additionally, it is less sensitive to measurement noise than the method based on the second HRR derivative.

Note that the results in Fig. 1, along with the accompanying discussion, already validated the methods underlying the assumption on symmetry of early and late combustion durations in autonomous HCCI. Figure 14 ultimately proves the validity of the proposed proprietary method for in-cycle designation of start of kinetic combustion in SACI. Figure 14 compares the results of $CA05_{HCCI}$ calculated using Eq. 8 (new method) and one determined using double Wiebe fitting (Eq. 3).

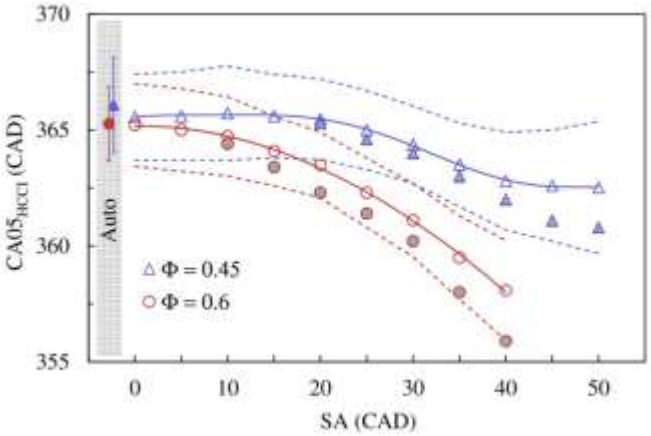

Fig. 14. $CA05_{HCCI}$ values estimated using double Wiebe method (filled in grey) and with the method based on CA50 and CA95 (empty points). Dashed lines show STDs at respective points. Filled points and error bars show CA05 values and STDs respectively for autonomous operation.

Note that the new method slightly overestimates $CA05_{HCCI}$. This deviation widens with increasing SA, correlated with the increasing amount of fuel burnt by flame propagation (Fig. 13). It is plausible, since high SI fractions provide greater acceleration to kinetic combustion. Nevertheless, the deviation in $CA05_{HCCI}$ estimation introduced by the new method, on a cycle-averaged basis, does not exceed 2 CAD (worst case), while adding cycle capability. The difference is within the STD of $CA05_{HCCI}$ calculated from individual cycles.

3.5. Cycle-to-cycle effects of flame propagation on kinetic combustion

In the preceding sections, we have identified relevant phenomena influencing CCV in HCCI and SACI. Apportionment of the fuel fractions associated to different combustion phases (Figs. 13 and 15) contributes towards understanding of variations in IMEP (Fig. 5) and individual combustion parameters (Figs. 8-10). Identification of the associated mechanisms requires a more comprehensive approach. This section focuses on the combustion in individual cycles and, using correlations validated in Section 3.4, aims to complement the existing knowledge on CCV in SACI and HCCI at the high-load transition boundary.

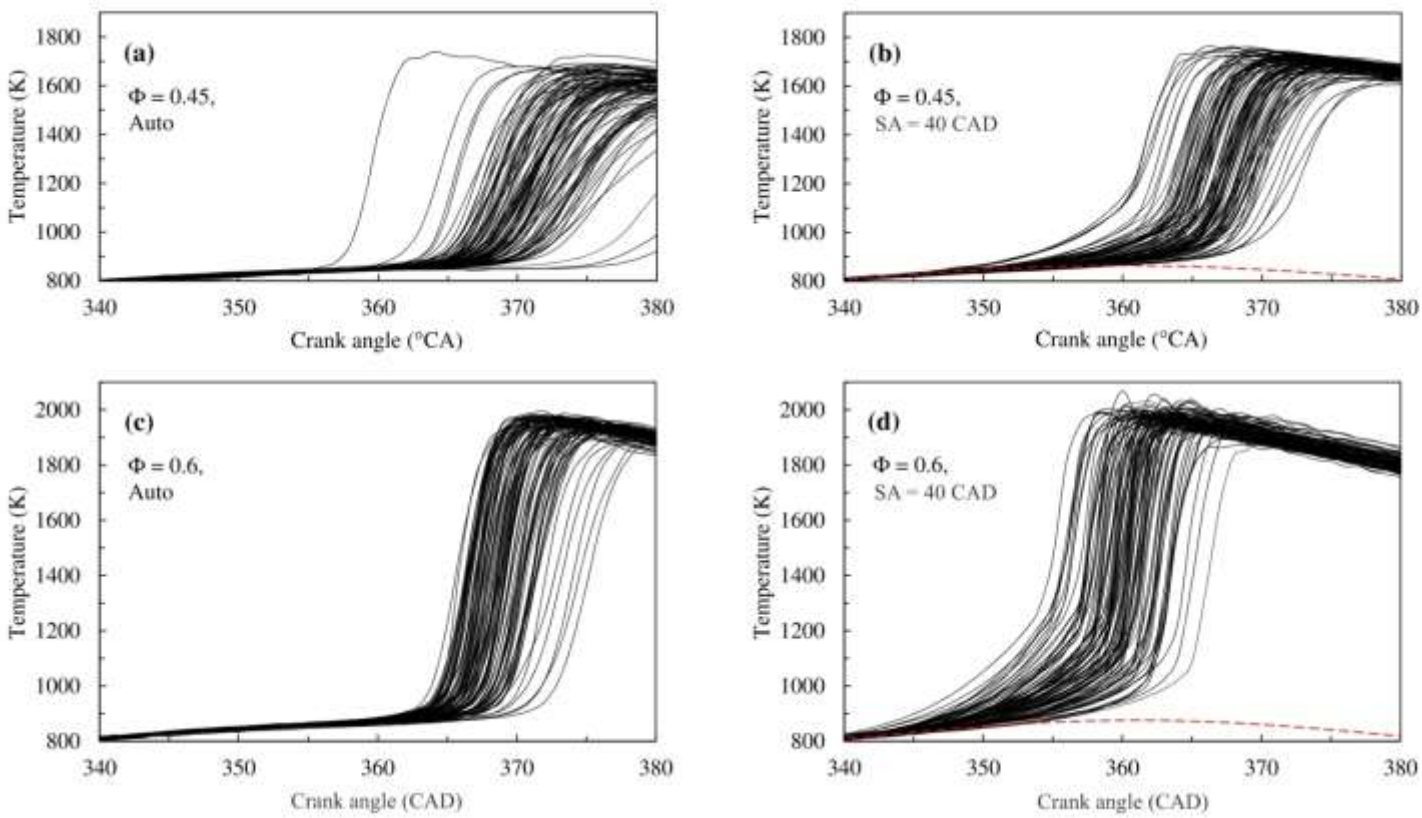

Fig. 15. In-cylinder temperature curves for 100 consecutive engine cycles; a) Φ = 0.45, autonomous, b) Φ = 0.45, SA = 40 CAD, c) Φ = 0.6, autonomous, d) Φ = 0.6, SA = 40 CAD. Red dashed lines show calculated polytropic compression temperatures, where starting point was average temperature at CASP.

From Fig. 12 we have identified that in-cylinder temperature development is a relevant parameter determining combustion timing. Figure 15 illustrates this coupling, using cycle-to-cycle temperature traces. For brevity, Fig. 15 compares autonomous HCCI and SACI at SA = 40 CAD at stoichiometric and lean conditions. As already noted, for lean mixture, autonomous HCCI results in high CVC. According to Fig. 15a, auto-ignition can occur as early as 357 CAD or as late as 375 CAD in lean conditions. These variations result from feedback coupling between consecutive combustion events. Late combustion produces a large amount of unburned hydrocarbons for the NVO phase. The fuel subjected to partial oxidation and reforming in the NVO-recompressed residuals increases temperature of the main event compression and plausibly enhances mixture reactivity, according to the mechanisms discussed in Hunicz et al. [40], [41]. The elevated thermal state and presence of highly reactive reformation products supports an early start in the forthcoming cycle, resulting in overall CCV. Adding spark discharge at lean conditions (Fig. 15b) clearly reduces CCV, both in terms of timing and peak temperature, where the driving force is reduction of late combustion cycles. At the same time, it is evident that the moment of rapid temperature rise

associated with the start of the kinetic combustion phase correlates with the temperature rise by the spark-initiated flame propagation. The greater the energy associated with the propagating flame, manifested in Fig. 15b as increased temperature before TDC (with respect to polytropic compression – red dashed line), then the earlier the kinetic phase starts. The amount of fuel burned by flame propagation is increased periodically by unburnt hydrocarbons from the preceding NVO cycle – the SACI CCV mechanism explained by Larimore et al. [30].

In the stoichiometric condition, CCV is already low for autonomous operation. This is evident in Fig. 15c. Thus, there are no overextended cycles to produce large variations in the cycle-available fuel, so CoV in IMEP remains roughly unchanged. STD of CA50 decreases slightly for the discussed SA = 20 CAD, since the cycles appear more focused. However, variability in combustion duration increases with further spark advance (Fig.10). The mechanism here is related to the additional variability in fractions undergoing flame propagation.

The coupling between the amount of energy released via flame propagation and start of kinetic phase is apparent when we overlay the results of $CA05_{HCCI}$ with individual cycle HRRs. Figure 16 shows this for the representative stoichiometric SACI points. The SA = 20 CAD, already discussed in Fig. 15, is the point where spark discharge actually reduces CCV with respect to homogenous baseline (see Fig. 5). On the other hand, for SA = 40 CAD, CCV significantly increases despite high SI fractions supporting ignition of the kinetic phase.

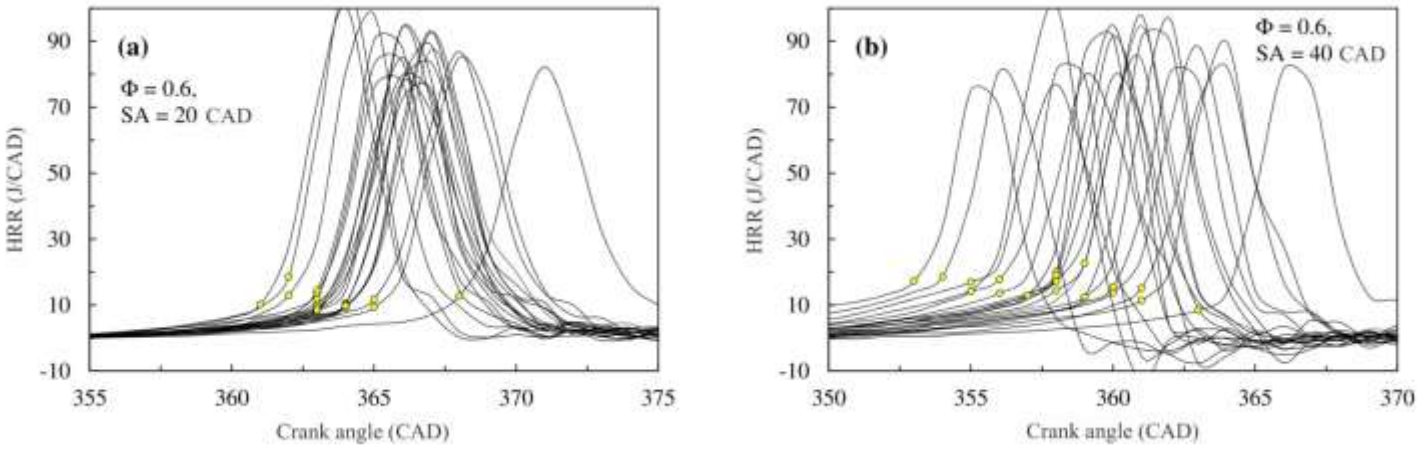

Fig. 16. Heat release rates for 20 consecutive engine cycles at Φ = 0.6; a) SA = 20 CAD, b) SA = 40 CAD. The yellow points indicate locations of $CA05_{HCCI}$.

According to Fig. 16, the $CA05_{HCCI}$ depends directly on intensity of the flame propagation phase. Short SA angles give small, yet controllable, flame propagation. There is a trade-off between spark assist´s stabilising effect on the kinetic phase and additional potential destabilisation caused by incontrollable flame propagation. Note that Fig. 13 suggests that on an average basis, SI fractions between 3 and 4% give the most stable SACI combustion, independent of the mixture conditions. Higher SI fractions are more prone to variations in this parameter, as evident from Fig 16.

The question arises, which parameter directly affects this intensity of flame propagation and hence the location of $CA05_{HCCI,}$ at different SA angles. To answer this question, the two parameters are bundled into one – the kinetic combustion delay ($CASP\text{-}05_{HCCI}$) defined as angular distance between spark discharge and $CA05_{HCCI}$. Figure 17 correlates $CASP\text{-}05_{HCCI}$ to cycle-specific temperature rise due to flame propagation. The latter is a delta between actual bulk temperature and polytropic compression temperature resulting from compression only (see Fig. 15 for reference). For presentation purposes, the reference CAs for which delta temperature are analysed were arbitrarily selected in accordance to observed trends. Namely, the middle column depicts the CA reference, where the most linear correlation between $CASP\text{-}05_{HCCI}$ and inverse of propagating flame temperature is observed. The left and right columns show correlations for CA locations shifted 4 CAD backwards and forwards.

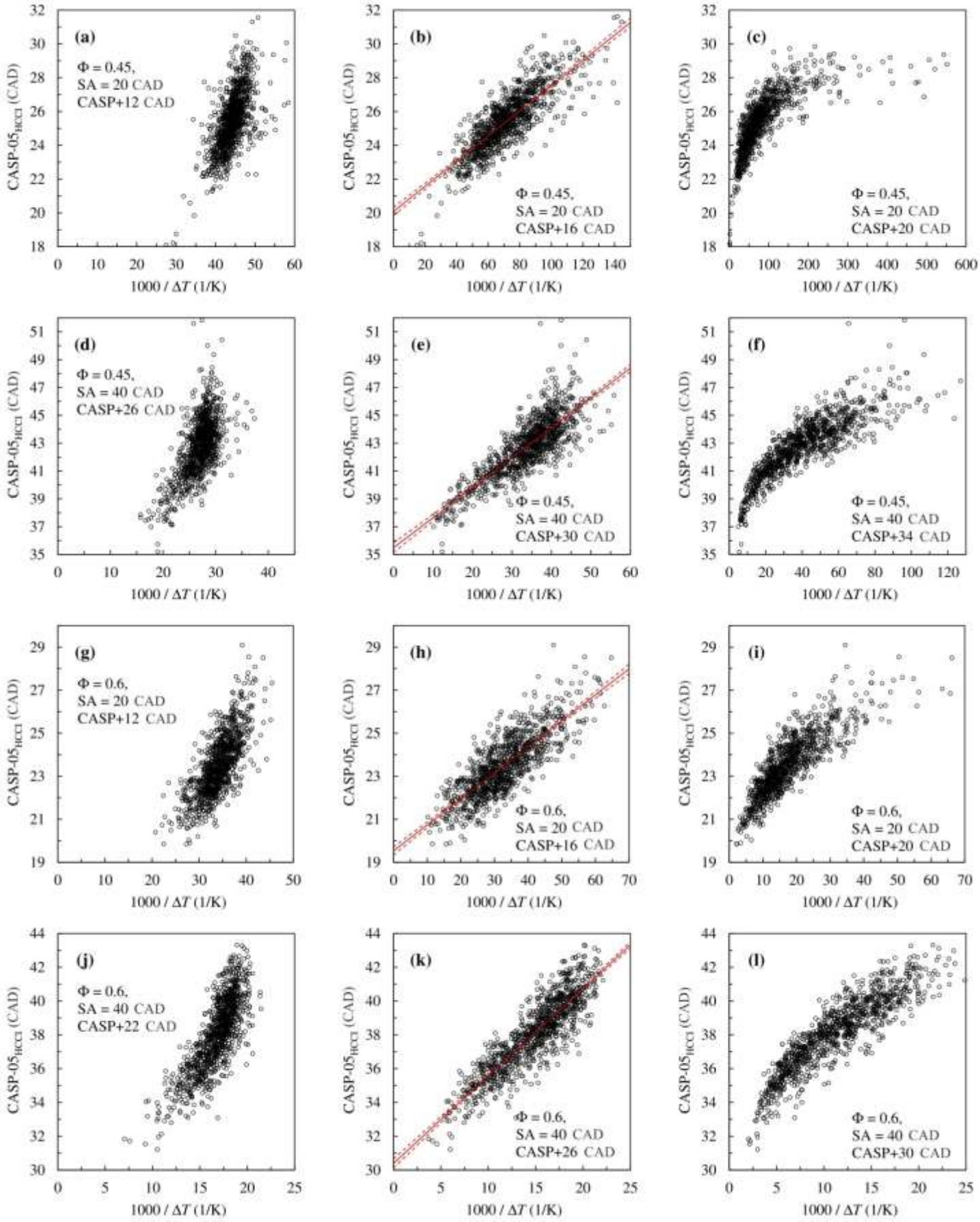
(a)
Φ = 0.45,
SA = 20 CAD
CASP+12 CAD
(b)
Φ = 0.45,
SA = 20 CAD
CASP+16 CAD
(c)
Φ = 0.45,
SA = 20 CAD
CASP+20 CAD
(d)
Φ = 0.45,
SA = 40 CAD
CASP+26 CAD
(e)
Φ = 0.45,
SA = 40 CAD
CASP+30 CAD
(f)
Φ = 0.45,
SA = 40 CAD
CASP+34 CAD
(g)
Φ = 0.6,
SA = 20 CAD
CASP+12 CAD
(h)
Φ = 0.6,
SA = 20 CAD
CASP+16 CAD
(i)
Φ = 0.6,
SA = 20 CAD
CASP+20 CAD
(j)
Φ = 0.6,
SA = 40 CAD
CASP+22 CAD
(k)
Φ = 0.6,
SA = 40 CAD
CASP+26 CAD
(l)
Φ = 0.6,
SA = 40 CAD
CASP+30 CAD
CASP-05HCCI (CAD)
1000 / ΔT (1/K)

Fig. 17. Calculated flame development durations (CASP-05_{HCCI}) as functions of inverted temperature rise at different angles after spark discharge.

Figure 17 proves that the bulk temperature rise due to flame propagation is the driving force for the auto-ignition phase in SACI. This further determines the overall combustion timing through $CA05_{HCCI}$ being bounded to CA50 and CA95 through Eq. 8. The correlation in Fig. 17 therefore can be used to provide in-cycle control to mitigate SACI CCV. The temperature rise can be real-time calculated from in-cylinder pressure analysis and the combustion timing estimated before the major fraction of fuel has burned. However, the locations for which regression is linear, enabling reliable prediction, depend on SA and mixture strength.

4. Discussions

The main takeaway from the previous section´s results is that monitoring in-cylinder pressure can reliably provide information on kinetic combustion timing. To this end, the method developed in this work for designating start of kinetic combustion, based on standard combustion indicators, is considered an enabler for overall combustion timing control.

This information could be used in control procedures to undertake some stabilisation actions, such as post injection of a small amount of fuel, which has advancing effect on combustion [51]. The stability achieved could extend the high-load operating range of SACI at lean mixtures, supporting low NO_X emissions and high efficiency. Before this is enabled however, further work is needed to find a specific condition for $CA05_{HCCI}$ to the temperature rise due to flame propagation. At this point, Fig. 17 only suggests that such a condition exists, but it could be identified with an analytical correlation with SA and mixture strength as additional arguments. Finding this correlation would require an extension of experiments, covering more mixture strengths and overall fuel values. Data-driven modelling like gene expression programming [52] could then be used to find the specific mathematical formulation.

In addition to proposing and verifying new methods of in-cycle combustion analysis, the present work makes several interesting observations regarding the SACI phenomena, which cannot be explained by means of traditional statistical combustion analysis. To this end, the deeper insight provided by the new approach enables us to answer the following research questions, set in Section 3.

(i) Why does CoV in IMEP, for both lean and stoichiometric SACI cases, have local minima for SA 25 CAD and SA 35 CAD respectively?

This was observed for the investigated cases in Fig 5. The phenomenon is confirmed by the clear effect on ISFC, which also minimises at the same SA set points, as seen in Fig. 6. The explanation is partially provided by Fig. 16´s discussion, outlining the trade-off between spark assist´s stabilising effect on the kinetic phase versus the additional destabilisation introduced by variations in spark-induced flame. Small fractions of flame propagation support controllable timing of the kinetic phase. On an averaged basis, the minimum CoV in IMEP for both operating points is reached for SAs that have SI fractions between 3% and 4%. Further increasing this fraction, by shifting SA towards earlier spark timings, leads to greater variability in fuel burned by flame propagation, translating into higher CoV in IMEP.

(ii) Why is the minimum CoV in IMEP not clearly reproduced by corresponding minimisation of standard deviations of combustion timing parameters?

Actually, the local minimum in CoV in IMEP seen in Fig. 5 is also present on the STD of CA50 (Fig. 8) and CA05 (Fig. 9). However, the reduction of variations of CA50 and CA05 is far less than for CoV in IMEP. The reason for this becomes clear when we look at the mechanism of how spark assist influences overall CCV. On one hand, adding spark discharge cuts down the incidence of late combustion cycles, which are characterised by heavily incomplete combustion. Naturally, the amount of fuel burned in the given cycle has a direct and more pronounced impact on IMEP than combustion timing – hence the clear reduction in CoV in IMEP. On the other hand, CoV in IMEP rises more rapidly for late SA because the overall acceleration of combustion timing means some cycles will oscillate closer to TDC. CA50 slightly before TDC will suppress IMEP rapidly because of the negative torque component: CA50 just after TDC maximises IMEP because it is the most efficient use of the cycle. Thus, when operating close to TDC, small variations in timing translate into greater CoV in IMEP.

(iii) What is the origin of CA50 sensitivity when switching from HCCI to SACI for lean mode?

Figure 8 indicates that there is a single degree advance of CA50 for spark discharge at TDC when compared to autonomous baseline. This happening even though flame development under such conditions is hardly noticeable (see Fig. 13 for reference). For comparison, the stoichiometric case, which was proven to support flame propagation, does not exhibit any sensitivity when switching from HCCI to SACI with spark discharge at TDC.

Although the mixture is too lean to ignite directly from the spark discharge before auto-ignition occurs, the additional energy introduced by the discharge slightly elevates the thermal state of the mixture, shaving off the late cycles. This effect is not noticeable under stoichiometric conditions because combustion itself is much more stable and there are no late cycles. This thesis is supported by detailed analysis of STD of CA50 (Fig. 8). For rich conditions STD is nearly the same for autonomous HCCI and SACI operation, but for the lean mixture, STD for autonomous combustion is approximately 1 CAD higher than for spark-assisted combustion.

The same mechanism explains the lean case´s insensitivity to late SAs. CA05 and CA50, together with their respective standard deviations, are unaffected by changes in spark advance between TDC (0 CAD) and 15 CAD. As long as no flame propagation is developing (Fig. 13), the energy delivered by the spark is the same for all SAs in the discussed range, so there is no effect on combustion timing.

5. Conclusions

Four main objectives underpin the premise of the present work. The main conclusion is that all objectives have been met, fulfilling the study´s goal to bridge the gap between fundamental and applied-level research in Spark Assisted Compression Ignition (SACI). To aid clarity, the following most relevant conclusions are matched to each of the four objectives set out in the introduction:

1. Combustion variability can be mitigated by applying spark assist. Operating lean SACI at high load, with 35 CAD spark advance, maintains high efficiency and ultra-low NO_X emissions (below 0.2 g/kWh), while keeping the acceptable trade-off between combustion variability (CoV in IMEP below 3%) and pressure rise rate (below 0.52 MPa/CAD).
2. In-cycle determination of transition point between flame propagation and kinetic phase is essential for controlling SACI combustion. The proposed new, real time-capable method is two orders of magnitude faster than the reference spline-Wiebe approach. Accuracy wise, a worst-case +/-2 CAD absolute error in kinetic phase prediction is associated with this calculation speed improvement.
3. Ability to determine the combustion regime change on the individual cycle basis discovers a trade-off between spark advance´s stabilising effect on the kinetic phase and additional destabilisation introduced by variations in spark-induced flame. Flame propagation fractions between 3% and 4% support minimum variations. Additionally, this discovery

allows explaining apparent inconsistencies observed in variations of individual combustion timing parameters.

4. The delay of kinetic combustion in SACI correlates well with temperature rise caused by flame propagation. The latter can be real-time calculated from in-cylinder pressure analysis. Combining this correlation with the developed method for determination of kinetic combustion onset paves the way towards predictive in-cycle control for SACI. However, more work is required to evaluate specific effects of spark advance and mixture strength.

Acknowledgments

The research was financed in the framework of the project: Lublin University of Technology – Regional Excellence Initiative, funded by the Polish Ministry of Science and Higher Education (contract no. 030/RID/2018/19).

References

[1] Reitz RD, Ogawa H, Payri R, Fansler T, Kokjohn S, Moriyoshi Y, et al. IJER editorial: The future of the internal combustion engine. International Journal of Engine Research 2020;21:3–10. doi:10.1177/1468087419877990.

[2] Pachiannan T, Zhong W, Rajkumar S, He Z, Leng X, Wang Q. A literature review of fuel effects on performance and emission characteristics of low-temperature combustion strategies. Applied Energy 2019. doi:10.1016/j.apenergy.2019.113380.

[3] Khobragade R, Singh SK, Shukla PC, Gupta T, Al-Fatesh AS, Agarwal AK, et al. Chemical composition of diesel particulate matter and its control. Catalysis Reviews - Science and Engineering 2019;61:447–515. doi:10.1080/01614940.2019.1617607.

[4] Lavy J, Dabadie J-C, Angelberger C, Duret P, Willand J, Juretzka A, et al. Innovative ultra-low NO_X controlled auto-ignition combustion process for gasoline engines: the 4-SPACE project. SAE Technical Paper 2000-01-1837, 2000. doi:10.4271/2000-01-1837.

[5] Haraldsson G, Tunestål P, Johansson B, Hyvönen J. HCCI Closed-Loop Combustion Control Using Fast Thermal Management. SAE Technical Paper 2004-01-0943, 2004. doi:10.4271/2004-01-0943.

[6] Puškár M, Kopas M. System based on thermal control of the HCCI technology developed for reduction of the vehicle NO_X emissions in order to fulfil the future standard Euro 7. Science of the Total Environment 2018;643:674–80.

doi:10.1016/j.scitotenv.2018.06.082.

[7] Pan M, Qian W, Wei H, Feng D, Pan J. Effects on performance and emissions of gasoline compression ignition engine over a wide range of internal exhaust gas recirculation rates under lean conditions. Fuel 2020;265. doi:10.1016/j.fuel.2019.116881.

[8] Li J, Zhao H, Ladommatos N, Ma T. Research and Development of Controlled Auto-Ignition (CAI) Combustion in a 4-Stroke Multi-Cylinder Gasoline Engine. SAE Technical Paper 2001-01-3608, 2001. doi:10.4271/2001-01-3608.

[9] Gorzelic P, Shingne P, Martz J, Stefanopoulou A, Sterniak J, Jiang L. A low-order adaptive engine model for SI-HCCI mode transition control applications with cam switching strategies. International Journal of Engine Research 2016;17:451–68. doi:10.1177/1468087415585016.

[10] Scaringe R, Wildman C, Cheng WK. On the High Load Limit of Boosted Gasoline HCCI Engine Operating in NVO Mode. SAE International Journal of Engines 2010;3:35–45. doi:10.4271/2010-01-0162.

[11] Saxena S, Bedoya ID. Fundamental phenomena affecting low temperature combustion and HCCI engines, high load limits and strategies for extending these limits. Progress in Energy and Combustion Science 2013;39:457–88. doi:10.1016/j.pecs.2013.05.002 Review.

[12] Hellström E, Stefanopoulou A, Vavra J, Babajimopoulos A, Assanis DN, Jiang L, et al. Understanding the Dynamic Evolution of Cyclic Variability at the Operating Limits of HCCI Engines with Negative Valve Overlap. SAE International Journal of Engines 2012;5:995–1008. doi:10.4271/2012-01-1106.

[13] Maurya RK, Agarwal AK. Experimental investigation on the effect of intake air temperature and air-fuel ratio on cycle-to-cycle variations of HCCI combustion and performance parameters. Applied Energy 2011;88:1153–63. doi:10.1016/j.apenergy.2010.09.027.

[14] Hunicz J. On cyclic variability in a residual effected HCCI engine with direct gasoline injection during negative valve overlap. Mathematical Problems in Engineering 2014;2014:359230. doi:10.1155/2014/359230.

[15] Ma H, Xu H, Wang J, Tan C. Investigation on the self-stabilization feature of HCCI combustion. SAE Technical Paper 2014-01-2663, 2014. doi:10.4271/2014-01-2663.

[16] Koopmans L, Backlund O, Denbratt I. Cycle to cycle variations: Their influence on cycle resolved gas temperature and unburned hydrocarbons from a camless gasoline

compression ignition engine. SAE Technical Paper 2002-01-0110, 2002. doi:10.4271/2002-01-0110.

[17] Hellström E, Larimore J, Stefanopoulou A, Sterniak J, Jiang L. Quantifying cyclic variability in a multicylinder HCCI engine with high residuals. Journal of Engineering for Gas Turbines and Power 2012;134. doi:10.1115/1.4007164.

[18] Ebrahimi R, Desmet B. An experimental investigation on engine speed and cyclic dispersion in an HCCI engine. Fuel 2010;89:2149–56. doi:10.1016/j.fuel.2010.04.005.

[19] Wolk B, Ekoto I, Northrop WF, Moshammer K, Hansen N. Detailed speciation and reactivity characterization of fuel-specific in-cylinder reforming products and the associated impact on engine performance. Fuel 2016;185:341–61. doi:10.1016/j.fuel.2016.07.103.

[20] Ratnak S, Kusaka J, Daisho Y, Yoshimura K, Nakama K. Effect of fuel injection timing during negative valve overlap period on a GDI-HCCI engine. ASME 2018 Internal Combustion Engine Division Fall Technical Conference, ICEF 2018 2018;1. doi:10.1115/ICEF2018-9653.

[21] Hunicz J, Geca M, Rysak A, Litak G, Kordos P. Combustion timing variability in a light boosted controlled auto-ignition engine with direct fuel injection. Journal of Vibroengineering 2013;15:1093–101.

[22] Ghazimirsaied A, Koch CR. Controlling cyclic combustion timing variations using a symbol-statistics predictive approach in an HCCI engine. Applied Energy 2012;92:133–46. doi:10.1016/j.apenergy.2011.09.018.

[23] Lawler B, Splitter D, Szybist J, Kaul B. Thermally Stratified Compression Ignition: A new advanced low temperature combustion mode with load flexibility. Applied Energy 2017;189:122–32. doi:10.1016/j.apenergy.2016.11.034.

[24] Wick M, Bedei J, Andert J, Lehrheuer B, Pischinger S, Nuss E. Dynamic measurement of HCCI combustion with self-learning of experimental space limitations. Applied Energy 2020;262. doi:10.1016/j.apenergy.2019.114364.

[25] Kalian N, Standing R, Zhao H. Effects of ignition timing on CAI combustion in a multi-cylinder di gasoline engine. SAE Technical Paper 2005-01-3720, 2005. doi:10.4271/2005-01-3720.

[26] Aleiferis PG, Charalambides AG, Hardalupas Y, Taylor AMKP, Urata Y. Autoignition initiation and development of n-heptane HCCI combustion assisted by inlet air heating, internal egr or spark discharge: An optical investigation. SAE Technical Paper 2006-01-3273, 2006. doi:10.4271/2006-01-3273.

[27] Persson H, Hultqvist A, Johansson B, Remón A. Investigation of the early flame development in spark assisted HCCI combustion using high speed chemiluminescence imaging. SAE Technical Paper 2007-01-0212, 2007. doi:10.4271/2007-01-0212.

[28] Chen T, Zhao H, Xie H, He B. Analysis of cyclic variations during mode switching between spark ignition and controlled auto-ignition combustion operations. International Journal of Engine Research 2015;16:356–65. doi:10.1177/1468087414555733.

[29] Daw CS, Wagner RM, Edwards KD, Green JB. Understanding the transition between conventional spark-ignited combustion and HCCI in argasoline engine. Proceedings of the Combustion Institute 2007;31 II:2887–94. doi:10.1016/j.proci.2006.07.133.

[30] Larimore J, Hellstrom E, Sterniak J, Jiang L, Stefanopoulou AG. Experiments and analysis of high cyclic variability at the operational limits of spark-assisted HCCI combustion. Proceedings of the American Control Conference, 2012, p. 2072–7. doi:10.1109/acc.2012.6315226.

[31] Ortiz-Soto EA, Lavoie GA, Martz JB, Wooldridge MS, Assanis DN. Enhanced heat release analysis for advanced multi-mode combustion engine experiments. Applied Energy 2014;136:465–79. doi:10.1016/j.apenergy.2014.09.038.

[32] Chang Y, Mendrea B, Sterniak J, Bohac S V. Effect of Ambient Temperature and Humidity on Combustion and Emissions of a Spark-Assisted Compression Ignition Engine. Journal of Engineering for Gas Turbines and Power 2017;139. doi:10.1115/1.4034966.

[33] Zhou L, Dong K, Hua J, Wei H, Chen R, Han Y. Effects of applying EGR with split injection strategy on combustion performance and knock resistance in a spark assisted compression ignition (SACI) engine. Applied Thermal Engineering 2018;145:98–109. doi:10.1016/J.APPLTHERMALENG.2018.09.001.

[34] Yıldız M, Albayrak Çeper B. Combustion development in a gasoline-fueled spark ignition–controlled auto-ignition engine operated at different spark timings and intake air temperatures. International Journal of Engine Research 2019. doi:10.1177/1468087419894165.

[35] ICE Breaker! 2017. https://www.sae.org/news/2017/09/ice-breaker (accessed May 22, 2020).

[36] German spark-ignited compression-ignition research paralleling Mazda's SPCCI 2018. https://www.sae.org/news/2018/04/saci-engine---sae-high-efficiency-engines-symposium (accessed May 22, 2020).

[37] Yamasaki Y, Umahashi S, Uesugi Y, Ma Q, Kaneko S, Hikita T, et al. Development of Dynamic Models for an HCCI Engine with Exhaust Gas Rebreathing System. SAE Technical Paper 2015-01-1803, 2015. doi:10.4271/2015-01-1803.

[38] Sen AK, Litak G, Edwards KD, Finney CEA, Daw CS, Wagner RM. Characteristics of cyclic heat release variability in the transition from spark ignition to HCCI in a gasoline engine. Applied Energy 2011. doi:10.1016/j.apenergy.2010.11.040.

[39] Kaul BC, Finney CE, Daw CS, Wagner RM, Edwards KD, Green JB. A review of deterministic effects in cyclic variability of internal combustion engines. International Journal of Engine Research 2015;16:366–78. doi:10.1177/1468087415572033.

[40] Hunicz J. An experimental study into the chemical effects of direct gasoline injection into retained residuals in a homogeneous charge compression ignition engine. International Journal of Engine Research 2016;17:1031–44. doi:10.1177/1468087416636492.

[41] Hunicz J, Mikulski M. Investigation of the thermal effects of fuel injection into retained residuals in HCCI engine. Applied Energy 2018;228:1966–84. doi:10.1016/j.apenergy.2018.07.075.

[42] Hunicz J. Cycle-by-cycle variations in autonomous and spark assisted homogeneous charge compression ignition combustion of stoichiometric air–fuel mixture. International Journal of Spray and Combustion Dynamics 2018;10:231–43. doi:10.1177/1756827718763564.

[43] Lapuerta M, Armas O, Hernández JJ. Diagnosis of DI Diesel combustion from in-cylinder pressure signal by estimation of mean thermodynamic properties of the gas. Applied Thermal Engineering 1999;19:513–29. doi:10.1016/S1359-4311(98)00075-1.

[44] Hohenberg GF. Advanced approaches for heat transfer calculations. SAE Technical Paper 790825, 1979. doi:10.4271/790825.

[45] Galindo J, Luján JM, Serrano JR, Hernández L. Combustion simulation of turbocharger HSDI Diesel engines during transient operation using neural networks. Applied Thermal Engineering 2005;25:877–98. doi:10.1016/j.applthermaleng.2004.08.004.

[46] Heywood JB. Internal combustion engine fundamentals. McGraw-Hill Education; 2018.

[47] Qu Z, Ravi N, Oudart J, Doran E, Mittal V, Kojic A. Control-oriented modeling of spark assisted compression ignition using a double Wiebe function. Proceedings of the American Control Conference, vol. 2015- July, 2015, p. 4741–6. doi:10.1109/ACC.2015.7172076.

[48] Hunicz J, Mikulski M, Geca MS, Rybak A. An applicable approach to mitigate pressure rise rate in an HCCI engine with negative valve overlap. Applied Energy 2020;257. doi:10.1016/j.apenergy.2019.114018.

[49] Lee C, Tomita E, Lee K. Characteristics of combustion stability and emission in SCCI and CAI combustion based on direct-injection gasoline engine. SAE Technical Paper 2007-01-1872, 2007. doi:10.4271/2007-01-1872.

[50] Manofsky Olesky L, Lavoie GA, Assanis DN, Wooldridge MS, Martz JB. The effects of diluent composition on the rates of HCCI and spark assisted compression ignition combustion. Applied Energy 2014;124:186–98. doi:10.1016/j.apenergy.2014.03.015.

[51] Hunicz J, Kordos P. An experimental study of fuel injection strategies in CAI gasoline engine. Experimental Thermal and Fluid Science 2011;35:243–52. doi:10.1016/j.expthermflusci.2010.09.007.

[52] Chakraborty A, Roy S, Banerjee R. Performance emission characterization of a LPG-diesel dual fuel operation: A gene expression programming approach. Advances in Intelligent Systems and Computing, vol. 741, 2019, p. 405–14. doi:10.1007/978-981-13-0761-4_39.